PHYSICAL REVIEW D **80,** 051103(R) (2009)

Measurements of charmless hadronic $b \to s$ penguin decays in the $\pi^+\pi^- K^+\pi^-$ final state and first observation of $B^0 \to \rho^0 K^+\pi^-$

S.-H. Kyeong,[48] Y.-J. Kwon,[48] I. Adachi,[8] H. Aihara,[44] A. M. Bakich,[40] V. Balagura,[14] E. Barberio,[22] A. Bay,[19] K. Belous,[12] M. Bischofberger,[24] A. Bozek,[28] M. Bračko,[21,15] T. E. Browder,[7] M.-C. Chang,[4] Y. Chao,[27] A. Chen,[25] B. G. Cheon,[6] C.-C. Chiang,[27] I.-S. Cho,[48] Y. Choi,[39] J. Dalseno,[8] A. Das,[41] A. Drutskoy,[2] W. Dungel,[11] S. Eidelman,[1,32] N. Gabyshev,[1,32] P. Goldenzweig,[2] H. Ha,[17] J. Haba,[8] B.-Y. Han,[17] T. Hara,[8] Y. Hasegawa,[38] K. Hayasaka,[23] H. Hayashii,[24] Y. Hoshi,[43] H. J. Hyun,[18] K. Inami,[23] A. Ishikawa,[35] R. Itoh,[8] M. Iwasaki,[44] N. J. Joshi,[41] D. H. Kah,[18] J. H. Kang,[48] P. Kapusta,[28] N. Katayama,[8] T. Kawasaki,[30] H. O. Kim,[18] J. H. Kim,[39] Y. I. Kim,[18] Y. J. Kim,[5] K. Kinoshita,[2] B. R. Ko,[17] S. Korpar,[21,15] P. Križan,[20,15] R. Kumar,[34] M. J. Lee,[37] T. Lesiak,[28,3] J. Li,[7] C. Liu,[36] Y. Liu,[23] R. Louvot,[19] A. Matyja,[28] S. McOnie,[40] K. Miyabayashi,[24] H. Miyata,[30] Y. Miyazaki,[23] R. Mizuk,[14] Y. Nagasaka,[9] E. Nakano,[33] M. Nakao,[8] Z. Natkaniec,[28] S. Nishida,[8] K. Nishimura,[7] O. Nitoh,[46] S. Ogawa,[42] T. Ohshima,[23] S. Okuno,[16] H. Ozaki,[8] P. Pakhlov,[14] G. Pakhlova,[14] C. W. Park,[39] H. Park,[18] H. K. Park,[18] R. Pestotnik,[15] L. E. Piilonen,[47] H. Sahoo,[7] K. Sakai,[30] Y. Sakai,[8] O. Schneider,[19] J. Schümann,[8] C. Schwanda,[11] A. J. Schwartz,[2] A. Sekiya,[24] K. Senyo,[23] M. E. Sevior,[22] M. Shapkin,[12] C. P. Shen,[7] J.-G. Shiu,[27] B. Shwartz,[1,32] J. B. Singh,[34] R. Sinha,[13] A. Sokolov,[12] S. Stanič,[31] M. Starič,[15] J. Stypula,[28] K. Sumisawa,[8] T. Sumiyoshi,[45] G. N. Taylor,[22] Y. Teramoto,[33] K. Trabelsi,[8] S. Uehara,[8] Y. Unno,[6] P. Urquijo,[22] G. Varner,[7] K. E. Varvell,[40] K. Vervink,[19] A. Vinokurova,[1,32] C. H. Wang,[26] M.-Z. Wang,[27] P. Wang,[10] Y. Watanabe,[16] R. Wedd,[22] E. Won,[17] B. D. Yabsley,[40] Y. Yamashita,[29] Z. P. Zhang,[36] V. Zhilich,[1,32] V. Zhulanov,[1,32] T. Zivko,[15] A. Zupanc,[15] and O. Zyukova[1,32]

(Belle Collaboration)

[1]*Budker Institute of Nuclear Physics, Novosibirsk*
[2]*University of Cincinnati, Cincinnati, Ohio 45221*
[3]*T. Kościuszko Cracow University of Technology, Krakow*
[4]*Department of Physics, Fu Jen Catholic University, Taipei*
[5]*The Graduate University for Advanced Studies, Hayama*
[6]*Hanyang University, Seoul*
[7]*University of Hawaii, Honolulu, Hawaii 96822*
[8]*High Energy Accelerator Research Organization (KEK), Tsukuba*
[9]*Hiroshima Institute of Technology, Hiroshima*
[10]*Institute of High Energy Physics, Chinese Academy of Sciences, Beijing*
[11]*Institute of High Energy Physics, Vienna*
[12]*Institute of High Energy Physics, Protvino*
[13]*Institute of Mathematical Sciences, Chennai*
[14]*Institute for Theoretical and Experimental Physics, Moscow*
[15]*J. Stefan Institute, Ljubljana*
[16]*Kanagawa University, Yokohama*
[17]*Korea University, Seoul*
[18]*Kyungpook National University, Taegu*
[19]*École Polytechnique Fédérale de Lausanne (EPFL), Lausanne*
[20]*Faculty of Mathematics and Physics, University of Ljubljana, Ljubljana*
[21]*University of Maribor, Maribor*
[22]*University of Melbourne, School of Physics, Victoria 3010*
[23]*Nagoya University, Nagoya*
[24]*Nara Women's University, Nara*
[25]*National Central University, Chung-li*
[26]*National United University, Miao Li*
[27]*Department of Physics, National Taiwan University, Taipei*
[28]*H. Niewodniczanski Institute of Nuclear Physics, Krakow*
[29]*Nippon Dental University, Niigata*
[30]*Niigata University, Niigata*
[31]*University of Nova Gorica, Nova Gorica*
[32]*Novosibirsk State University, Novosibirsk*
[33]*Osaka City University, Osaka*
[34]*Panjab University, Chandigarh*
[35]*Saga University, Saga*

[36]*University of Science and Technology of China, Hefei*
[37]*Seoul National University, Seoul*
[38]*Shinshu University, Nagano*
[39]*Sungkyunkwan University, Suwon*
[40]*University of Sydney, Sydney, New South Wales*
[41]*Tata Institute of Fundamental Research, Mumbai*
[42]*Toho University, Funabashi*
[43]*Tohoku Gakuin University, Tagajo*
[44]*Department of Physics, University of Tokyo, Tokyo*
[45]*Tokyo Metropolitan University, Tokyo*
[46]*Tokyo University of Agriculture and Technology, Tokyo*
[47]*IPNAS, Virginia Polytechnic Institute and State University, Blacksburg, Virginia 24061*
[48]*Yonsei University, Seoul*

(Received 6 May 2009; published 4 September 2009)

We report measurements of charmless hadronic B^0 decays into the $\pi^+\pi^-K^+\pi^-$ final state. The analysis uses a sample of 657×10^6 $B\bar{B}$ pairs collected with the Belle detector at the KEKB asymmetric-energy e^+e^- collider at the resonance. The decay $B^0 \to \rho^0 K^+\pi^-$ is observed for the first time; the significance is 5.0σ and the corresponding partial branching fraction for $M_{K\pi} \in (0.75, 1.20)$ GeV/c^2 is $[2.8 \pm 0.5(\text{stat}) \pm 0.5(\text{syst})] \times 10^{-6}$. We also obtain the first evidence for $B^0 \to f_0(980)K^+\pi^-$ with 3.5σ significance and for $B^0 \to \pi^+\pi^-K^{*0}$ with 4.5σ significance. For the two-body decays $B^0 \to \rho^0 K^{*0}$ and $B^0 \to f_0(980)K^{*0}$, the significances are 2.7σ and 2.5σ, respectively, and the upper limits on the branching fractions are 3.4×10^{-6} and 2.2×10^{-6} at 90% confidence level.

DOI: 10.1103/PhysRevD.80.051103 PACS numbers: 13.25.Hw, 11.30.Er, 14.40.Nd

In the standard model (SM), charmless hadronic B meson decays occur mainly via two processes: (i) $b \to sq\bar{q}$ transitions mediated by penguin diagrams, and (ii) $b \to uW^*$ transitions mediated by tree diagrams. These diagrams as they pertain to $B^0 \to \rho^0 K^{*0}$ [1], for example, are shown in Fig. 1. Both of these processes are suppressed relative to the more common $b \to cW^*$ decays due to either (i) the one-loop structure or (ii) the small ratio of Cabibbo-Kobayashi-Maskawa matrix [2] elements $|V_{ub}/V_{cb}|$, respectively. Because of this suppression, these decays are especially sensitive to non-SM contributions [3].

There have been several puzzling results from measurements of charmless hadronic B decays. For example, B decays to $K^+\pi^-$ and $K^+\pi^0$ show different patterns of direct CP violation [4], which are inconsistent with naïve SM expectations. It has been suggested [5] that vector-vector (VV) final states with the same quark combinations, e.g. $B \to \rho K^*$ may give insights to this puzzle, as any difference between $K\pi$ and their VV counterparts will be mainly hadronic. In addition, charmless B decays to VV final states show intriguing results in the final-state polarizations. The decays $B \to \phi K^*$ and $B \to \rho K^*$, both occurring mostly via the $b \to s$ penguin process, are found to have large transverse polarizations [6–8], in contrast to the expectation from factorization. On the other hand, $B^{+(0)} \to \rho^+\rho^{0(-)}$, which is mostly a $b \to uW^*$ tree-diagram process, is almost fully polarized longitudinally [9]. There have been theoretical [5,10] studies of these modes, in part focusing on the final-state polarizations within and beyond the SM.

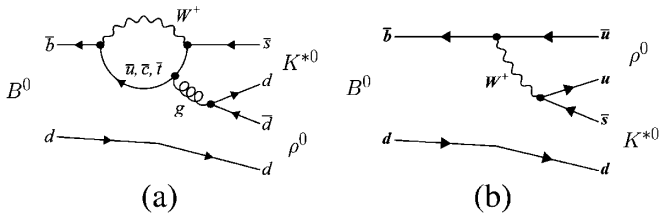

FIG. 1. Feynman diagrams for charmless hadronic B decays pertaining to $B^0 \to \rho^0 K^{*0}$: (a) $b \to s$ penguin diagram, and (b) $b \to u$ tree diagram.

One difficulty in measuring charmless $B \to VV$ decays, however, is that nonresonant decays to the same final state can be a significant background [11]. Such nonresonant decays may have different decay properties, e.g., different polarization of the vector mesons. While there are several experimental studies of B^0 decays to the $\pi^+\pi^-K^+\pi^-$ final state [7,12], there is no experimental information on the nonresonant components of these final states.

In this paper, we analyze charmless hadronic decays of B^0 to the $\pi^+\pi^-K^+\pi^-$ final state. We search for two-body final states such as $B^0 \to \rho^0 K^{*0}$ and $f_0(980)K^{*0}$, and also for three-body states $\rho^0 K^+\pi^-$, $f_0(980)K^+\pi^-$ [13], and $\pi^+\pi^-K^{*0}$, where the $\pi^+\pi^-$ or $K^+\pi^-$ pairs are nonresonant. A comprehensive understanding of these decays with a clear distinction between nonresonant and two-body resonant decays would advance our understanding of strong and weak interaction dynamics.

We use a data sample containing 657×10^6 $B\bar{B}$ pair events collected with the Belle detector [14] at the KEKB [15] asymmetric-energy e^+e^- collider (3.5 on 8 GeV),

operating at the $\Upsilon(4S)$ resonance. To reconstruct $B^0 \to \pi^+\pi^- K^+\pi^-$ decays including the intermediate states $\rho^0 \to \pi^+\pi^-$, $f_0(980) \to \pi^+\pi^-$, and $K^{*0} \to K^+\pi^-$, we select four charged tracks of which two are positively charged and two are negatively charged. Each track is required to originate within 5.0 cm of the interaction point along the beam direction, and within 0.2 cm of the interaction point in the transverse plane [8]. We also require that the transverse momentum of each track be larger than 0.1 GeV/c [8]. Tracks identified as electrons are rejected. We identify charged kaons and pions by combining particle identification (PID) information obtained from the central drift chamber, the time-of-flight system, and the aerogel Cherenkov counters [16].

Signal candidates are selected for further analysis based on four kinematic variables: the $\pi^+\pi^-$ and $K^+\pi^-$ invariant masses ($M_{\pi\pi}$ and $M_{K\pi}$), the energy difference $\Delta E \equiv E_B - E_{\rm beam}$, and the beam-energy-constrained mass $M_{\rm bc} \equiv \sqrt{E^2_{\rm beam} - p^2_B}$, where $E_{\rm beam}$ is the beam energy and E_B and p_B are the energy and momentum, respectively, of the candidate B meson. These variables are all evaluated in the $\Upsilon(4S)$ c.m. frame. We retain events satisfying $|\Delta E| < 0.1$ GeV, $5.24\ \text{GeV}/c^2 < M_{\rm bc} < 5.29\ \text{GeV}/c^2$, $0.55\ \text{GeV}/c^2 < M_{\pi\pi} < 1.20\ \text{GeV}/c^2$, and $0.75\ \text{GeV}/c^2 < M_{K\pi} < 1.20\ \text{GeV}/c^2$. To optimize the background suppression criteria, tighter "signal regions" are defined for $M_{\rm bc}$ and ΔE: $5.27\ \text{GeV}/c^2 < M_{\rm bc} < 5.29\ \text{GeV}/c^2$ and $|\Delta E| < 0.045$ GeV. The fraction of events having multiple candidates is approximately 20%. For multiple-candidate events, we select the candidate decay having the smallest χ^2 from the B vertex fit. Given a set of four particles, $\pi^+\pi^- K^+\pi^-$, two combinations of $(\pi^+\pi^-)$ and $(K^+\pi^-)$ may lie inside the selected mass ranges. In this case, which occurs in less than 1% of signal decays, we pair the higher-momentum π^- with the π^+.

The dominant source of background is from continuum $e^+e^- \to q\bar{q}$ events ($q = u$, d, s, and c). These events are distinguished from the signal by their event shape. Since B mesons are spinless and produced nearly at rest in the c.m. frame, their daughter particles are distributed almost isotropically. On the other hand, continuum events usually produce two back-to-back jets in the c.m. frame. We use Monte Carlo (MC) simulated [17] signal events and sideband data ($5.20\ \text{GeV}/c^2 < M_{\rm bc} < 5.26\ \text{GeV}/c^2$) for optimizing the continuum suppression requirements. First we form a Fisher discriminant $\mathcal{F}$ based on a set of modified Fox-Wolfram moments [18]. These moments are uncorrelated with the four kinematical variables mentioned above. Two more variables are used for continuum suppression: $\cos\theta_B$, the cosine of the polar angle of the B flight direction in the c.m. frame; and Δz, the displacement along the beam direction between the vertex of the signal B and that of the other B in the event. Likelihood functions for signal ($\mathcal{L}_s$) and continuum background ($\mathcal{L}_{q\bar{q}}$) are formed from products of the probability density functions (PDFs) for $\mathcal{F}$, $\cos\theta_B$, and Δz. These are combined into a likelihood ratio $\mathcal{R}_{q\bar{q}} = \mathcal{L}_s/(\mathcal{L}_s + \mathcal{L}_{q\bar{q}})$. To obtain improved continuum suppression, we optimize the requirement on $\mathcal{R}_{q\bar{q}}$ as a function of flavor-tagging information from the accompanying B meson. The Belle flavor-tagging algorithm [19] yields the b-flavor variable q ($= \pm 1$), and the quality variable r. The latter ranges from zero for no flavor discrimination to one for unambiguous flavor assignment. We optimize the $\mathcal{R}_{q\bar{q}}$ requirement independently in six bins of qr. For $B^0 \to \rho^0 K^{*0}$, for example, the optimized $\mathcal{R}_{q\bar{q}}$ requirements remove 99% of the $q\bar{q}$ background while retaining 42% of the signal.

B decays to a charm meson (D^0 or $D^{(*)+}$) and multiple pions constitute a significant background that exhibits peaking behavior in $M_{\rm bc}$ and ΔE similar to that of the signal. To eliminate this background, we veto candidates that have a $K\pi\pi$, $K\pi$, or $\pi\pi$ invariant mass consistent with a $D^{(*)+} \to K^-\pi^+\pi^+$, $D^0 \to K^-\pi^+$, and $D^0 \to \pi^-\pi^+$ decay, respectively.

The signal yields are obtained from a four-dimensional extended unbinned maximum-likelihood [20] fit (4D fit) to $M_{\rm bc}$, ΔE, $M_{\pi\pi}$, and $M_{K\pi}$. The likelihood function is

$$\mathcal{L} \equiv \frac{\exp(-\sum Y_j)}{N!} \prod_{i=1}^{N} \sum_j Y_j \mathcal{P}^i{}_j, \qquad (1)$$

where Y_j is the yield of the jth component, $\mathcal{P}^i{}_j$ is the PDF value for the jth component of the ith event, and i runs over all events in the fit region (N). We include 13 components in Eq. (1): B^0 decays to $\rho^0 K^{*0}$, $f_0(980)K^{*0}$, and $f_2(1270)K^{*0}$; the nonresonant components $\rho^0 K^+\pi^-$, $f_0(980)K^+\pi^-$, $\pi^+\pi^- K^{*0}$, and $\pi^+\pi^- K^+\pi^-$; the feed-down components $a_1^-(1260)K^+$, $K_1^+(1270)\pi^-$, and $K_1^+(1400)\pi^-$; and background components from $q\bar{q}$ continuum ($q\bar{q}$), charmed B decays ($b \to c$), and charmless B decays ($b \to s$, u, and d).

The PDFs for the signal are separated into two categories: correctly reconstructed events and self-cross-feed (SCF) events. The SCF events include at least one track that is taken from the accompanying B meson decay. For correctly reconstructed events, a sum of two Gaussians with a common mean is used for the $M_{\rm bc}$ and ΔE shapes. The $M_{\pi\pi}$ and $M_{K\pi}$ distributions are modeled by relativistic Breit-Wigner functions. The ρ^0, $f_2(1270)$, and K^{*0} resonance parameters are fixed to their PDG values [21]. Parameters of the $f_0(980)$ resonance shape are fixed to the results of Ref. [22]; these values have higher precision than the corresponding PDG values. PDFs for the SCF components are modeled using kernel estimation [23] of SCF MC distributions. For the $M_{\pi\pi}$ and $M_{K\pi}$ PDFs of nonresonant components, a threshold function and/or Chebyshev polynomials are used. The $M_{\rm bc}$ and ΔE shapes for the signal PDFs are calibrated using a large $B^0 \to D^-\pi^+$, $D^- \to K^+\pi^-\pi^-$ control sample, to take into ac-

count small differences observed between MC-simulated events and data.

The PDF shapes of the $q\bar{q}$ background are modeled with an ARGUS [24] function for $M_{\rm bc}$, linear functions for ΔE, and combinatorial shapes for $M_{\pi\pi}$ and $M_{K\pi}$. For $b \to c$ background, the PDFs are obtained separately for correctly reconstructed K^{*0} and for random $K\pi$ combinations. The fraction of each component is fixed from the MC simulation. The PDF shapes for $b \to s$, u, and d background are modeled with nonparametric PDFs using kernel estimation [23].

The following parameters are floated in the 4D fit: the yields of the signal modes (given in Table I) and background yields of $b \to c$ and $q\bar{q}$; the parameters of the $q\bar{q}$ PDF describing the $M_{\rm bc}$, ΔE and combinatorial shapes of $M_{\pi\pi}$ and $M_{K\pi}$. The branching fractions of the feed-down components are fixed to the results of Ref. [25]. The yield of $f_2(1270)K^{*0}$ is fixed to 43.0 events as obtained from two-dimensional $M_{\rm bc}$-ΔE fitting in bins of $M_{\pi\pi}$ as discussed later. The remaining parameters are fixed to values obtained from MC simulations.

The fit projections are shown in Fig. 2, and the results are summarized in Table I. There are moderate correlations between some modes, which we check by fitting an ensemble of GEANT-simulated MC samples. We find a negligible effect on the measured signal yields. The branching fraction of each mode is determined by $\mathcal{B} = Y/(\varepsilon_{\rm MC}\varepsilon_{\rm PID}N_{B\bar{B}})$, where Y is the fitted signal yield, $\varepsilon_{\rm MC}$ is the event selection efficiency including daughter branching fractions as obtained from MC simulation, and $\varepsilon_{\rm PID}$ is an efficiency correction ($\varepsilon_{\rm PID} = 0.96$) for PID that accounts for small differences between MC and data. The production rates of $B^0\bar{B}^0$ and B^+B^- pairs are assumed to be equal.

The fit yields the first observation for $B^0 \to \rho^0 K^+\pi^-$ with a significance of 5.0σ. The significance is defined as $\sqrt{-2\ln(\mathcal{L}_0/\mathcal{L}_{\rm max})}$, where $\mathcal{L}_0$ ($\mathcal{L}_{\rm max}$) is the value of the likelihood function when the yield is fixed to zero (allowed to vary). We include systematic uncertainties by smearing the likelihood function with a Gaussian whose width is equal to the systematic uncertainty (discussed below). We also find evidence for $B^0 \to f_0(980)K^+\pi^-$ with a significance of 3.5σ, and evidence for $B^0 \to \pi^+\pi^- K^{*0}$ with a significance of 4.5σ. For $B^0 \to \rho^0 K^{*0}$ and $B^0 \to f_0(980)K^{*0}$, we observe excesses of events with significances of 2.7σ and 2.5σ, respectively. For the nonresonant decay components, the $\mathcal{B}$ and $\varepsilon_{\rm MC}$ values correspond to the ranges $M_{K\pi} \in (0.75, 1.20)$ GeV/c^2, $M_{\pi\pi} \in (0.55, 1.20)$ GeV/c^2, and assume three-body phase space distributions. For modes with less than 3σ significance, we also list a 90% confidence level (C.L.) upper limit (UL). This limit is determined via

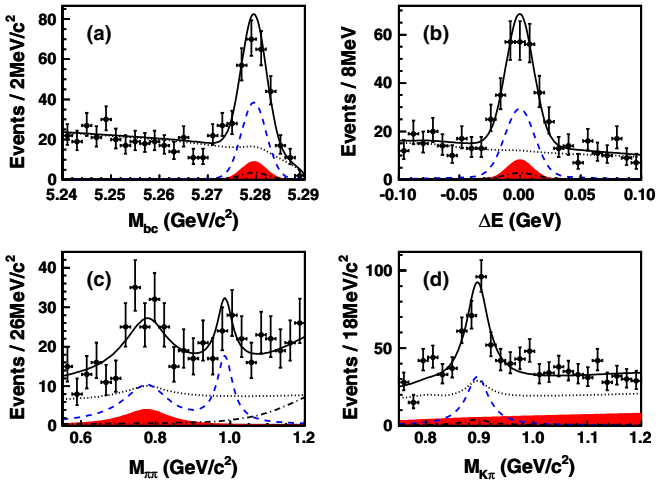

FIG. 2 (color online). Projection of the 4D fit results onto (a) $M_{\rm bc}$, (b) ΔE, (c) $M_{\pi\pi}$, and (d) $M_{K\pi}$, with the other variables required to satisfy (except for the variable plotted) $M_{\rm bc} \in (5.27, 5.29)$ GeV/c^2, $\Delta E \in (-0.045, 0.045)$ GeV, $M_{\pi\pi} \in (0.62, 1.04)$ GeV/c^2, and $M_{K\pi} \in (0.84, 0.94)$ GeV/c^2. The curves are for the $\rho^0 K^+\pi^-$ (solid shaded regions), the sum of $\rho^0 K^{*0}$ and $f_0(980)K^{*0}$ (dashed lines), $f_2(1270)K^{*0}$ and the sum of feed-down modes (dot-dashed lines), the sum of the backgrounds (dotted lines), and the total (solid lines).

TABLE I. The signal yield Y and its statistical uncertainty, corrected MC efficiency ε (assuming $f_L = 0.5$ for $B^0 \to \rho^0 K^{*0}$), significance $\mathcal{S}$ including the systematic uncertainties, measured branching fraction $\mathcal{B}$, and the UL at the 90% confidence level $\mathcal{B}_{\rm UL}$. For nonresonant decay components, ε, $\mathcal{B}$, and $\mathcal{B}_{\rm UL}$ are obtained for $M_{K\pi} \in (0.75, 1.20)$ GeV/c^2 and $M_{\pi\pi} \in (0.55, 1.20)$ GeV/c^2 assuming phase space distributions. For the branching fraction, the first (second) uncertainty is statistical (systematic).

Mode	Y (events)	ε (%)	$\mathcal{S}$ (σ)	$\mathcal{B}$ (10^{-6})	$\mathcal{B}_{\rm UL}$ (10^{-6})
$\rho^0 K^{*0}$	$77.6^{+28.6}_{-27.9}$	5.73	2.7	$2.1^{+0.8+0.9}_{-0.7-0.5}$	<3.4
$f_0(980)K^{*0}$	$51.2^{+20.4}_{-19.3}$	5.56	2.5	$1.4^{+0.6+0.6}_{-0.5-0.4}$	<2.2
$\rho^0 K^+\pi^-$	$207.8^{+39.8}_{-39.2}$	11.15	5.0	$2.8 \pm 0.5 \pm 0.5$	$\cdots$
$f_0(980)K^+\pi^-$	$106.9^{+31.6}_{-29.9}$	11.43	3.5	$1.4 \pm 0.4^{+0.3}_{-0.4}$	<2.1
$\pi^+\pi^- K^{*0}$	$200.7^{+46.7}_{-44.9}$	6.74	4.5	$4.5^{+1.1+0.9}_{-1.0-1.6}$	$\cdots$
$\pi^+\pi^- K^+\pi^-$	$-5.4^{+54.9}_{-44.9}$	6.84	0.0	$-0.1^{+1.2+1.4}_{-1.1-0.8}$	<2.1

TABLE II. Summary of systematic uncertainties (%) in the efficiency (ε) determination.

Source	ρK^*	fK^*	$\rho K\pi$	$fK\pi$	$\pi\pi K^*$	$\pi\pi K\pi$
MC statistics	± 0.5	± 0.7	± 1.3	± 1.7	± 1.3	± 2.1
Tracking	± 4.2	± 4.2	± 4.2	± 4.2	± 4.2	± 4.2
PID	± 3.7	± 3.7	± 3.7	± 3.8	± 3.8	± 3.7
$\mathcal{R}_{q\bar{q}}$ cut	± 3.4	± 3.4	± 3.4	± 3.4	± 3.4	± 3.4
$N_{B\bar{B}}$	± 1.4	± 1.4	± 1.4	± 1.4	± 1.4	± 1.4
$f_{\rm L}$	$^{+16.7}_{-18.9}$	...	...	...	...	...
Sum	$^{+18.0}_{-20.1}$	± 6.7	± 6.8	± 7.0	± 6.9	± 7.0

$$\frac{\int_0^{\mathcal{B}_{\rm UL}} \mathcal{L}(\mathcal{B})d\mathcal{B}}{\int_0^{\infty} \mathcal{L}(\mathcal{B})d\mathcal{B}} = 90\%. \quad (2)$$

The sources and sizes of systematic uncertainties in the efficiency determination and the yield extraction are summarized in Tables II and III, respectively. The main sources of efficiency uncertainties are tracking (4.2%), PID (3.7%–3.8%), MC sample statistics (0.5%–2.1%), and the $\mathcal{R}_{q\bar{q}}$ requirement (3.4%). Table II also includes the uncertainty from $N_{B\bar{B}}$ (1.4%). While this does not affect the efficiency determination, it leads to a multiplicative uncertainty in $\mathcal{B}$. An additional uncertainty in the efficiency for $B^0 \to \rho^0 K^{*0}$ arises from the unknown fraction of longitudinal polarization ($f_{\rm L}$). For our central value, we take $f_{\rm L} = 0.5$ and estimate the uncertainty by considering the two extreme cases $f_{\rm L} = 0$ and $f_{\rm L} = 1$. The systematic uncertainties in the yield extraction are obtained by varying all fixed parameters of the PDFs by $\pm 1\sigma$, feed-down yields by $\pm 3\sigma$, and the fractions of SCF and $b \to s, u, d$ backgrounds by $\pm 50\%$, respectively. We consider the effects of higher K^{*0} resonances by including a PDF for $B^0 \to \rho^0 K_0^*(1430)^0$ and repeating the 4D fit with its yield floated by extending the fitting region in $M_{K\pi}$ to 1.5 GeV/c^2; the resulting changes are included as a systematic uncertainty.

We study the effects of possible interference among ρ^0, $f_0(980)$, $f_2(1270)$, and nonresonant $\pi^+\pi^-$ modes by including interference terms with variable phases in the $M_{\pi\pi}$ relativistic Breit-Wigner function. The effect is estimated by refitting with this modified PDF; the resulting shifts in the yields are included in the systematic uncertainties. We obtain the systematic uncertainty due to possible interference between K^{*0}, $K_0^*(1430)^0$, and nonresonant $K^+\pi^-$ in the $M_{K\pi}$ mass spectrum in a similar manner. Uncertainties due to a possible fitting bias are determined using a large sample of MC-simulated events. We assign the small biases found in the MC simulation as systematic uncertainties.

To verify the large contribution from nonresonant components (see Table I), we study background-subtracted $M_{\pi\pi}$ and $M_{K\pi}$ spectra. These spectra are obtained by binning the data in $M_{\pi\pi}$ or $M_{K\pi}$ and, for each bin, fitting the two-dimensional $M_{\rm bc}$-ΔE distribution to determine the sum of resonant and nonresonant yields. Figure 3 shows these yields as a function of $M_{\pi\pi}$ and $M_{K\pi}$. Relativistic Breit-Wigner functions are used as PDF's for the resonances with their parameters fixed to their PDG values [21]. The PDFs for the nonresonant contributions are modeled by threshold functions using MC-simulated events.

In summary, we have made the first observation of the three-body decay $B^0 \to \rho^0 K^+ \pi^-$ with 5.0σ significance and obtained the first evidence for nonresonant $B^0 \to f_0(980)K^+\pi^-$ and $B^0 \to \pi^+\pi^- K^{*0}$ decays. The corresponding partial branching fractions are measured. For the $B^0 \to \rho^0 K^{*0}$ and $B^0 \to f_0(980)K^{*0}$ modes, we find approximately 2.6σ signal excesses and obtain the results listed in Table I. Our result for these two-body decays are 2σ and 1σ lower, respectively, than in the previous measurement [7]. We have also searched for the fully nonresonant four-body decay $B^0 \to \pi^+\pi^- K^+\pi^-$ and calculated a 90% C.L. upper limit on its partial branching fraction. Our results for the nonresonant modes are the first such results and may help us understand the polarization puzzle in ρK^* decays. With additional $B \to VV$ data, these measurements can be used to constrain models of new physics [26].

We thank the KEKB group for excellent operation of the accelerator, the KEK cryogenics group for efficient sole-

TABLE III. Summary of systematic uncertainties (events) in the signal yield (Y) extraction.

Source	ρK^*	fK^*	$\rho K\pi$	$fK\pi$	$\pi\pi K^*$	$\pi\pi K\pi$
Fitting PDFs	$^{+4.4}_{-5.4}$	$^{+12.7}_{-11.8}$	$^{+5.8}_{-9.1}$	$^{+24.1}_{-23.6}$	$^{+18.1}_{-17.4}$	$^{+29.4}_{-27.9}$
$f_{f_2(1270)K^{*0}}$	$^{+11.0}_{-11.3}$	$^{+5.9}_{-6.4}$	$^{+0.3}_{-0.3}$	$^{+0.3}_{-0.1}$	$^{+13.9}_{-13.7}$	$^{+30.0}_{-35.4}$
$f_{\rm feed\text{-}down}$	$^{+0.6}_{-1.4}$	$^{+0.1}_{-0.1}$	$^{+4.7}_{-1.5}$	$^{+0.3}_{-0.4}$	$^{+8.7}_{-3.8}$	$^{+3.2}_{-1.9}$
$f_{b\to s,u,d}$	$^{+1.9}_{-2.1}$	$^{+0.1}_{-0.0}$	$^{+7.0}_{-9.8}$	$^{+0.3}_{-0.4}$	$^{+0.0}_{-1.2}$	$^{+3.7}_{-0.8}$
$f_{\rm SCF}$	$^{+2.1}_{-2.1}$	$^{+1.2}_{-1.2}$	$^{+19.9}_{-20.6}$	$^{+7.4}_{-7.3}$	$^{+8.2}_{-8.3}$	$^{+11.8}_{-11.4}$
$K_0^*(1430)^0$	$^{+29.0}_{-0.0}$	$^{+14.7}_{-0.0}$	$^{+16.9}_{-12.4}$	$^{+0.0}_{-19.3}$	$^{+0.0}_{-54.8}$	$^{+69.1}_{-0.0}$
Fitting bias	$^{+2.7}_{-0.0}$	$^{+4.9}_{-0.0}$	$^{+11.2}_{-0.0}$	$^{+0.0}_{-10.2}$	$^{+0.0}_{-26.6}$	$^{+0.0}_{-29.9}$
Interference	$^{+6.6}_{-5.6}$	$^{+2.3}_{-0.9}$	$^{+14.7}_{-17.3}$	$^{+4.3}_{-0.0}$	$^{+3.8}_{-3.6}$	...
Sum	$^{+31.5}_{-12.2}$	$^{+20.5}_{-12.3}$	$^{+34.8}_{-31.3}$	$^{+25.6}_{-32.9}$	$^{+35.5}_{-69.8}$	$^{+76.2}_{-42.6}$

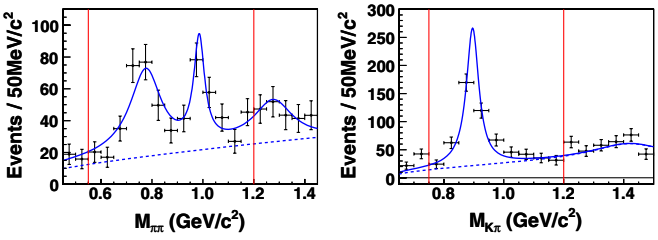

FIG. 3 (color online). Signal yields obtained from the two-dimensional fits to $M_{\rm bc}$ and ΔE in bins of $M_{\pi\pi}$ (left panel) and $M_{K\pi}$ (right panel) up to the higher-mass regions. Solid curves show the results of the two-dimensional binned fit, and dashed curves show the contributions of nonresonant $\pi^+\pi^-$ (left panel) and the sum of nonresonant $K^+\pi^-$ and $K_0^*(1430)^0$ (right panel). The vertical lines show the nominal 4D fit regions.

noid operations, and the KEK computer group and the NII for valuable computing and SINET3 network support. We acknowledge support from MEXT, JSPS, and Nagoya's TLPRC (Japan); ARC and DIISR (Australia); NSFC (China); DST (India); MEST, KISTI, and NRF (Korea); MNiSW (Poland); MES and RFAAE (Russia); ARRS (Slovenia); SNSF (Switzerland); NSC and MOE (Taiwan); and DOE (USA). S.-H. K. acknowledges support by the Seoul Science program. Y.-J. K. acknowledges support by NRF Grant No. 2009-0077003.

[1] Throughout this paper, charge-conjugate processes are implied unless explicitly stated otherwise.
[2] M. Kobayashi and T. Maskawa, Prog. Theor. Phys. **49**, 652 (1973); N. Cabibbo, Phys. Rev. Lett. **10**, 531 (1963).
[3] See, for example, A. J. Buras and R. Fleischer, Eur. Phys. J. C **16**, 97 (2000); Y. Y. Keum, H. N. Li, and A. I. Sanda, Phys. Rev. D **63**, 054008 (2001).
[4] S.-W. Lin *et al.* (Belle Collaboration), Nature (London) **452**, 332 (2008); B. Aubert *et al.* (*BABAR* Collaboration), Phys. Rev. Lett. **99**, 021603 (2007).
[5] M. Beneke *et al.*, Phys. Rev. Lett. **96**, 141801 (2006); C. S. Kim *et al.*, Phys. Rev. D **76**, 074019 (2007).
[6] B. Aubert *et al.* (*BABAR* Collaboration), Phys. Rev. D **78**, 092008 (2008); ()Phys. Rev. Lett. **99**, 201802 (2007); K.-F. Chen *et al.* (Belle Collaboration), Phys. Rev. Lett. **94**, 221804 (2005).
[7] B. Aubert *et al.* (*BABAR* Collaboration), Phys. Rev. Lett. **97**, 201801 (2006).
[8] J. Zhang *et al.* (Belle Collaboration), Phys. Rev. Lett. **95**, 141801 (2005).
[9] B. Auber *et al.* (*BABAR* Collaboration), Phys. Rev. Lett. **102**, 141802 (2009); Phys. Rev. D **76**, 052007 (2007); A. Somov *et al.* (Belle Collaboration), Phys. Rev. Lett. **96**, 171801 (2006); J. Zhang *et al.* (Belle Collaboration), Phys. Rev. Lett. **91**, 221801 (2003).
[10] M. Beneke *et al.*, Nucl. Phys. **B774**, 64 (2007); H. W. Huang *et al.*, Phys. Rev. D **73**, 014011 (2006); S. Baek *et al.*, Phys. Rev. D **72**, 094008 (2005); M. Ladisa *et al.*, Phys. Rev. D **70**, 114025 (2004); S. Oh, Phys. Rev. D **60**, 034006 (1999).
[11] P. Goldenzweig *et al.* (Belle Collaboration), Phys. Rev. Lett. **101**, 231801 (2008); C.-C. Chiang *et al.* (Belle Collaboration), Phys. Rev. D **78**, 111102 (2008).
[12] B. Aubert *et al.* (*BABAR* Collaboration), Phys. Rev. D **76**, 071104 (2007); W. Adam *et al.* (DELPHI Collaboration), Z. Phys. C **72**, 207 (1996).
[13] In this paper, we assume a branching fraction of 100% for $f_0(980) \to \pi^+\pi^-$.
[14] A. Abashian *et al.* (Belle Collaboration), Nucl. Instrum. Methods Phys. Res., Sect. A **479**, 117 (2002).
[15] S. Kurokawa and E. Kikutani, Nucl. Instrum. Methods Phys. Res., Sect. A **499**, 1 (2003), and other papers in this volume.
[16] E. Nakano, Nucl. Instrum. Methods Phys. Res., Sect. A **494**, 402 (2002).
[17] Evtgen generator, D. J. Lange, Nucl. Instrum. Methods Phys. Res., Sect. A **462**, 152 (2001). The detector response is simulated with GEANT, R. Brun *et al.*, GEANT 3.21, CERN Report No. DD/EE/84-1, 1984.
[18] S. H. Lee *et al.* (Belle Collaboration), Phys. Rev. Lett. **91**, 261801 (2003).
[19] H. Kakuno *et al.*, Nucl. Instrum. Methods Phys. Res., Sect. A **533**, 516 (2004).
[20] L. Lyons, *Statistics for Nuclear and Particle Physicists* (Cambridge University Press, Cambridge, England, 1986).
[21] C. Amsler *et al.* (Particle Data Group), Phys. Lett. B **667**, 1 (2008).
[22] T. Mori *et al.* (Belle Collaboration), Phys. Rev. D **75**, 051101 (2007).
[23] K. Cranmer, Comput. Phys. Commun. **136**, 198 (2001).
[24] H. Albrecht *et al.* (ARGUS Collaboration), Phys. Lett. B **241**, 278 (1990).
[25] B. Aubert *et al.* (*BABAR* Collaboration), Phys. Rev. Lett. **100**, 051803 (2008); F. Blanc *et al.* (*BABAR* Collaboration), in Proceedings of the IVIIth Rencontres de Moriond: QCD and High Energy Hadronic Interactions, La Thulie, 2007.
[26] M. Beneke *et al.*, Eur. Phys. J. C **61**, 429 (2009).